IOP PUBLISHING FLUID DYNAMICS RESEARCH

Fluid Dyn. Res. **42** (2010) 035501 (23pp) doi:10.1088/0169-5983/42/3/035501

Molecular dynamics simulations of nanodroplet spreading on solid surfaces, effect of droplet size

Nahid Sedighi[1], **Sohail Murad**[2] **and Suresh K Aggarwal**[1,3]

[1] Department of Mechanical and Industrial Engineering, University of Illinois at Chicago, Chicago, IL, USA
[2] Department of Chemical Engineering, University of Illinois at Chicago, Chicago, IL, USA

E-mail: ska@uic.edu

Received 20 July 2009, in final form 3 November 2009
Published 28 January 2010
Online at stacks.iop.org/FDR/42/035501

Communicated by H J Sung

Abstract

Molecular dynamics simulations were performed to study the spreading characteristics of nano-sized droplets on solid surfaces. The spreading behavior was analyzed in terms of the temporal evolution of the dynamic contact angle and spreading diameter for wettable, partially wettable and non-wettable surfaces. The computational model was validated through qualitative comparison with the measurements of Bayer and Megaridis, and through comparison with existing correlations. The comparison based on the ratio of relevant time scales indicated that for the conditions investigated, the spreading dynamics is governed by inertial and surface forces, with negligible influence of viscous forces. In addition, the simulation results indicated that the dynamic contact angle and spreading diameter, as well as the advancing and receding time periods, exhibit strong dependence on droplet size. These results were further analyzed to obtain correlations for the effect of droplet size on these spreading parameters. The correlations indicated that the normalized spreading diameter and contact angle scale with drop diameter as $D_m/D_0 \propto D_0^{0.5}$ and $\theta_R \propto D_0^{0.5}$, while the advancing and receding time periods scale as $t \propto D_0^{2/3}$. Global kinetic energy and surface energy considerations were used to provide a physical basis for these correlations. The correlations were also found to be generally consistent with the experimentally observed spreading behavior of macroscopic droplets.

(Some figures in this article are in colour only in the electronic version)

[3] Author to whom any correspondence should be addressed.

0169-5983/10/035501+23$30.00

1. Introduction

Spreading of droplets on solid surfaces is important in a wide variety of applications, including propulsion, industrial surface coating, spray painting, spray cooling, ink-jet printing, agricultural sprays and biological sensors. In coating applications, a spatially uniform coating requires fundamental understanding of the mechanisms that influence the spreading dynamics. Similarly in agricultural sprays, the objective is to cover a foliar surface with the desired material as fast and uniformly as possible. In many propulsion applications, the wall impingement of liquid droplets often determines the fuel vapor distribution and thereby the combustion and emission characteristics. In spray cooling, the droplet spreading has a strong influence on the heat transfer characteristics.

Inkjet printing involves droplet deposition on a moving or stationary surface (Pede *et al* 1998, Choi *et al* 2004, Boland *et al* 2007) and is used in numerous applications, including desktop printing, electronic circuitry for generating conductive tracks and electronic components, and printing transparent coatings and thin films for transistors, solar cells and displays (Lee *et al* 2007). It is also used for printing proteins, DNA and cells in medical devices. Inkjet printing is a key technology in microelectronics and fabrication of micro and nano devices. In microelectronics, metallic conducting tracks are produced by depositing a series of droplets, containing an organo-metallic compound (or metal nanoparticles) dissolved in a carrier fluid, on a moving substrate (Lee and Kim 2000). As the droplet spreads on the surface, the carrier fluid evaporates and the organo-metallic compound (or nanoparticles) is deposited, forming a metallic track. The quality, lateral resolution and morphological properties of the track formed strongly depend on the droplet spreading dynamics (Graham-Rowe 2007), while the track width depends on the equilibrium contact angle. Important parameters affecting the wetting behavior include the liquid viscosity and surface tension, droplet size and velocity, droplet and surface temperatures, substrate speed and surface wettability.

Characterizing the dynamic spreading behavior has been very challenging, as it involves scales ranging from continuum to molecular, and the relevant parameters, such as Weber number (*We*) and capillary number (*Ca*), can vary over a wide range (Hoffman 1975, Blake 2006). Moreover, it has a wide variety of applications, involving different fluids and substrates, which further adds to the complexity. A common quantity used to characterize dynamic spreading is the contact angle of the moving wetting line, or the dynamic contact angle $\theta(t)$ (Yarin 2006). From a macroscopic view, the forced spreading is governed by the inertial and surface forces, and the dynamic contact angle decreases rapidly, while the spreading diameter increases during the early stages of spreading. The dynamic contact angle during this stage (advancing stage) is significantly different from the equilibrium value. This is followed by the second stage characterized by a slow change in the contact angle, as it approaches its equilibrium value. On the other hand, for instantaneous droplet spreading, the dynamic wetting process is governed by the capillary and viscous forces, as the contact angle decreases from its initial value of 180° to its equilibrium value θ_{E}.

Experimental studies concerning droplet spreading have focused on characterizing the spreading behavior as a function of important parameters (*We*, *Ca*, etc), and determining the dynamic and equilibrium contact angles as well as the maximum spreading ratio (D_{m}/D_0), which is defined as the ratio of the maximum droplet diameter during spreading to the original diameter. These studies generally employed mm-size droplets and various imaging techniques to capture droplet deformation following its impact on a given substrate. Accordingly, a number of correlations has been developed to quantify the effects of *We*, *Ca* and other parameters on the spreading characteristics (Pasandideh-Fard *et al* 1996, Aziz and

Chandra 2000, Crooks *et al* 2001, Sikalo *et al* 2002, Bathel *et al* 2007). Several of these correlations are listed in Bathel *et al* (2007).

Theoretical studies have generally followed two approaches to describe the dynamic spreading phenomenon and provide correlations for the temporal variation of the spreading diameter and contact angle as well as the relationship between dynamic contact angle and slip line velocity. The first approach is based on the hydrodynamic theory (Tanner 1979, Cox 1986, Shikhmurzaev 1997, Blake 2006) that considers droplet spreading from a continuum viewpoint. It employs an appropriate model to account for molecular processes in the microscopic layer in the vicinity of the moving contact line, and to provide a relationship between the macroscopic and microscopic contact angles. In order to avoid the shear stress singularity at the contact line, the no-slip boundary condition is appropriately modified by using different slip conditions (Bayer and Megaridis 2006). Theoretical and computational studies here have employed simplified analysis based on the force and energy balance (Yang 1975, Chandra and Avedisian 1991, Asai *et al* 1993, Scheller and Bousfield 1995, Mao *et al* 1997) as well as on the solution of the appropriate Navier-Stokes equations (Zhao *et al* 1996, Delplanque and Rangel 1997) to obtain correlations for the effects of important parameters (*We*, *Ca*, etc) on spreading characteristics. The second approach employs a molecular-kinetic theory (Blake and Haynes 1969, Cherry and Holmes 1969), which postulates that the macroscopic wetting behavior is determined by the overall statistics of the individual molecular displacements occurring within the three-phase zone. Thus, the contact line motion occurs due to the jumping of molecules from the liquid to the vapor side of the contact line, and its velocity is determined by the frequency κ and length λ of the individual molecular displacements. Shikhmurzaev (1997) presents a unifying model combining the two approaches. Blake (2006) provides an elegant discussion of these models and the related experimental studies concerning the validation of the models.

Clearly, the phenomenon of droplet spreading on solid substrates has been extensively investigated, and good phenomenological understanding and numerous correlations have been developed. However, mechanisms associated with the contact line motion and dynamic spreading are still not well understood (Dussan 1979, de Gennes 1985, Cazabat *et al* 1990). Moreover, a unifying approach to describe the dynamics of spreading in different systems is not yet available (De Coninck *et al* 2001). This may partly be attributed to the wide range of scales associated with the dynamic spreading processes, and experimental difficulties in capturing the spreading dynamics especially for droplet sizes in the sub-mm range. For example, for a drop-on-demand inkjet system, the advancing stage lasts less than 100 μs for micron-size droplets (Dong *et al* 2006). While high-speed imaging techniques have provided much useful information (Attinger *et al* 2000, Kim *et al* 2003, Van Dam and Le Clerc 2004), they have not yielded time-resolved measurements for such droplet sizes. Moreover, our literature review indicates that while the dynamic wetting behavior at the continuum scale has been extensively investigated, relatively few studies have been reported dealing with nano-sized droplets.

In the present study, we have performed molecular dynamics (MD) simulations to investigate the dynamic spreading behavior of nano-size droplets impinging on flat surfaces with different wetting characteristics. The major objective is to examine the effect of droplet size on spreading dynamics, characterized in terms of the temporal variations of contact angle and spreading diameter, as well as the advancing and receding time periods. Previous investigations using MD simulations (Heslot *et al* 1989, Cazabat *et al* 1990, Yang *et al* 1991, De Coninck *et al* 1995, Voue *et al* 1998a, 1998b; de Ruijter *et al* 1999, Heine *et al* 2003) have not examined these aspects. For example, the study by Voue *et al* focuses on the film diffusion rate as a function of the solid–fluid interaction potentials. Their results show agreement with

Table 1. System properties used in MD simulations.

D_0				$N_{\text{Particles}}$			
(nm)	ε_w	ε_f	Box dim. [σ]	Total	Drop	Surface	Ambient
6	1, 0.15, 0.05	1.0	$34.9 \times 34.9 \times 69.8$	5553	2123	2440	990
9	1, 0.15, 0.05	1.0	$52.4 \times 52.4 \times 104.8$	21232	7011	10920	3301
12	1, 0.15, 0.05	1.0	$69.8 \times 69.8 \times 139.7$	44048	16757	19360	7931

experiments, which found non-monotonic dependence of the diffusion rate on the strength of the fluid–solid interaction. The simulations reported a maximum value for intermediate strengths of solid–fluid interactions. For high strength interactions, the fluid structure mimics the solid structure, and that limits the diffusion rates. In our previous study (Sedighi *et al* 2009), an efficient algorithm was developed to track the liquid-phase interface and the dynamic contact angle for a liquid droplet in contact with two solid surfaces. This algorithm is used to investigate the droplet spreading dynamics in the present study. The numerical model is validated by qualitatively and semi-quantitatively comparing our simulations with the measurements of Bayer and Megaridis (2006). Simulations are then used to examine the dynamic spreading behavior, and the effects of surface wettability and droplet size on the spreading characteristics. In the next two sections, we describe the simulation model and its validation. This is followed by the discussion of results on the effects of droplet size on spreading dynamics, and the scaling relationships. Conclusions are presented in the last section.

2. Computational model

We examined the spreading behavior of nano-sized liquid argon droplets on solid surfaces using MD simulations. The simulation system is a 3D box that consists of 44 048 argon atoms[4], which constitute the liquid droplet, solid surface and ambient gas atoms. The interactions between molecules were represented by the Lennard-Jones (LJ) potential

$$\phi(r) = 4\varepsilon[(\sigma/r)^{12} - (\sigma/r)^{6}], \tag{1}$$

where σ and ε are the characteristic length and energy parameters of the LJ potential. The potential was truncated at a cut-off distance of 3σ, as is usual in such models (Allen and Tildesley 1987). For argon atoms, $\varepsilon = 1.67 \times 10^{-21}$ J and $\sigma = 3.405$ Å. The dimensions of the simulation box and the values of various parameters used in simulations are provided in table 1. The liquid density and temperature are $0.75\,\sigma^{-3}$ and $0.72\,\varepsilon/k$, respectively. The fluid particles can move freely in the 3D system and periodic boundary conditions are employed at the system boundaries. For the result shown, we used $\rho_f = 0.75\sigma^{-3}$ for the droplet. The surrounding (ambient) gas had an initial density of $\rho_a = 0.0167\rho_f$, and the reduced initial temperature was $T^* = kT/\varepsilon = 0.72$. Note that the subscripts f, a and w denote, respectively, the droplet fluid, ambient fluid and wall (surface).

The surface–surface interactions were also modeled with the LJ potential. Each wall atom was attached to the lattice site with a simple harmonic potential, with a spring constant of $K = 100\varepsilon/\sigma^2$, and is allowed to oscillate due to thermal fluctuations around its lattice position. The equations of motion were integrated using Gear's fifth order predictor–corrector algorithm. The time step is $\Delta t = 0.005\tau = 1.078 \times 10^{-2}$ ps, where $\tau = (m\sigma^2/\varepsilon)^{1/2}$ with m the mass of an argon atom. Note that all variables reported here are normalized with respect to argon parameters ($\varepsilon = 1.67 \times 10^{-21}$ J, $\sigma = 3.405$ Å and $m = 39.948$ amu). The system was

[4] This value corresponds to the 12 nm droplet case.

initialized for approximately 500 time steps. The coordinates of all molecules were sampled every 500 steps for subsequent analysis. The droplet initially has a spherical shape, and is placed at the geometric center of the surface with an initial velocity of $1.25\,\mathrm{m\,s^{-1}}$. The impact velocity was chosen to allow us to observe key steps of the spreading phenomena. The droplet is allowed impinge on the surface and then spread. The spreading is influenced by both the magnitude of initial impact velocity and the interaction between the liquid/surface/vapor molecules.

Several sets of MD simulations were performed to examine the effect of droplet size on the dynamic spreading behavior. Three droplets with diameters of 6, 9 and 12 nm have been considered. The wetting and spreading of each droplet is examined on surfaces with high to low surface energies. This variation resulted in three different surfaces, wettable ($\theta_e < 40$), partially wettable $40 < \theta_e < 140$ and non-wettable ($\theta_e > 140$). Here θ_e represents the equilibrium or static contact angle. The system parameters used in our simulations are listed in table 1. Here ε_w is the reduced interaction energy of the surface with respect to liquid, i.e. $\varepsilon_w^* = \varepsilon_w/\varepsilon_f$ where for simplicity from hereon the asterisk is removed and it is written as ε_w.

After the initial impact of the droplet with the surface, we observed rapid radial spreading, resulting in the flattening and recoiling of the drop. To investigate the dynamics of droplet spreading and contact angle evolution, an algorithm was developed to track the interface and compute the contact angle using density profiles. The liquid–vapor interface was defined when the density is approximately 25% of the bulk liquid value. This interface was then used to compute contact angle (slope of the curve passing through the interfacial points). As discussed by Sedighi *et al* (2009), the uncertainty in the calculation of contact angle is generally less than 10%. The spreading diameter and time evolution of spreading were monitored at different stages of the spreading process.

3. Results and discussion

3.1. Model validation and dynamics of spreading

In order to validate the computational model, we compared our simulation results with measurements of Bayer and Megaridis (2006) for the impact of a 1.4 mm water droplet on flat surfaces with different wetting characteristics. Note that the comparison is qualitative due to different conditions in simulations and measurements. Consequently, the comparison of spreading characteristics presented in figures 1 and 2 provides reasonable justification rather than validation for the computational model. The impact velocity in their study was $0.77\,\mathrm{m\,s^{-1}}$. Figure 1 shows images from our simulation at various times for the dynamic spreading of a 6 nm droplet on wettable ($\varepsilon = 1$), partially wettable ($\varepsilon = 0.15$) and non-wettable ($\varepsilon = 0.05$) surfaces. Figure 2 presents the corresponding images from the cited study. While there are significant quantitative differences between simulations and measurements due to the vastly different conditions, there is also striking similarity between them. The simulations are able to reproduce the overall spreading behavior observed experimentally for all three surfaces. Based on the images presented in figures 1 and 2, and the temporal evolution of spreading diameter in figure 3, the overall spreading process can be divided into two stages: an advancing stage during which the droplet base expands and the spreading diameter increases rapidly to nearly its maximum value, followed by a receding stage[5] during which the droplet base shrinks, i.e. the contact diameter decreases (Starov *et al* 2002). The spreading behavior during these two stages is well captured by simulations, although there are

[5] The receding stage is not observed for the wettable case (cf figures 1–3). This is also consistent with the observations of Starov *et al* (2002).

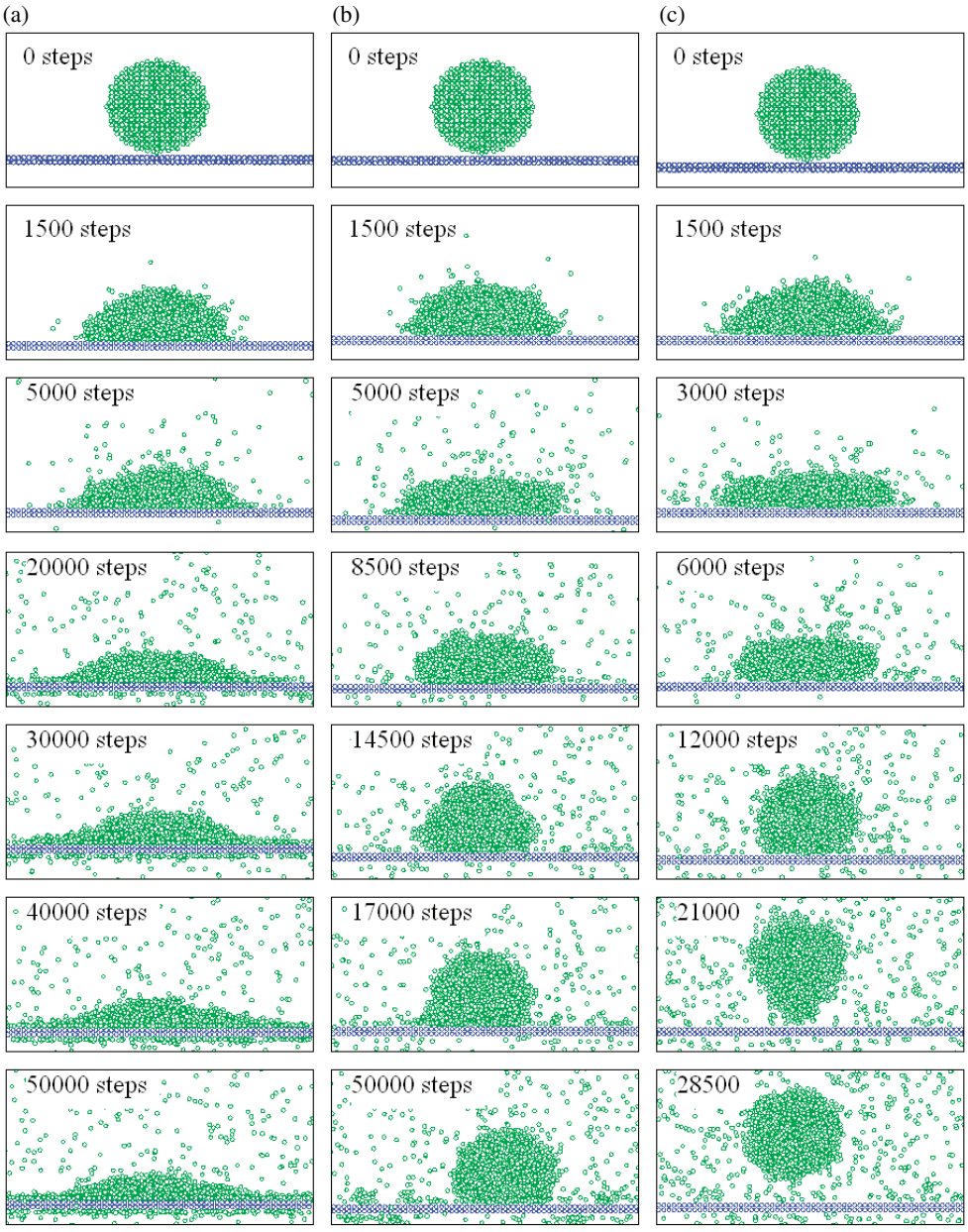

Figure 1. Spreading dynamics of a 6 nm droplets with initial velocity $V_0 = 1.25\,\mathrm{m\,s^{-1}}$ on three flat surfaces with different wetting properties: (a) wettable surface, $\varepsilon_w = 1.0$, (b) partially wettable, $\varepsilon_w = 0.15$ and (c) non-wettable, $\varepsilon_w = 0.05$.

differences between simulations and experiments with respect to the droplet shape at different times. For the non-wettable surface, the receding stage is followed by the droplet bouncing off from the surface. The bounce-off is also well captured by simulations, as indicated by a comparison of the images in figures 1 and 2, and of the temporal variation of spreading diameters for the non-wettable case in figure 3.

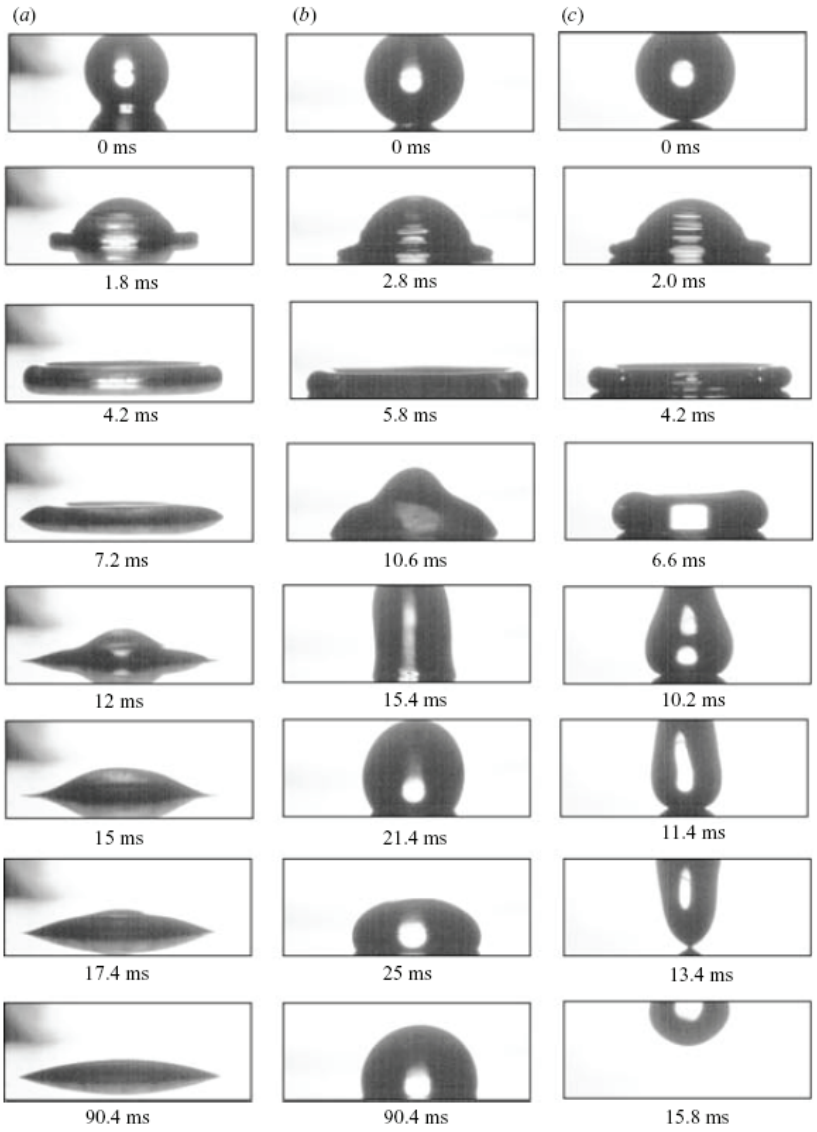

Figure 2. Spreading dynamics of 1.4 mm water droplets with $V_0 = 0.7\,\mathrm{m\,s^{-1}}$ on three flat surfaces with different degrees of wetting: (a) wettable, (b) partially wettable and (c) non-wettable. Taken from Bayer and Megaridis (2006).

There are other notable similarities between simulations and experiments. Firstly, both the simulations and experiments indicate that for an inertial impact, the spreading process during the advancing stage and the variation of D_m/D_0 are relatively insensitive to the surface wetting properties. This can be seen in the first three images from the simulations and experiments for all the three surfaces (cf figures 1 and 2), as well as from the temporal variation of D_m/D_0 in figure 3. Secondly, for the wettable surface, the spreading process following the advancing stage is characterized by a slow relaxation to equilibrium whereby the spreading diameter remains nearly constant or increases at a very slow rate, as indicated in figures 1–3, while

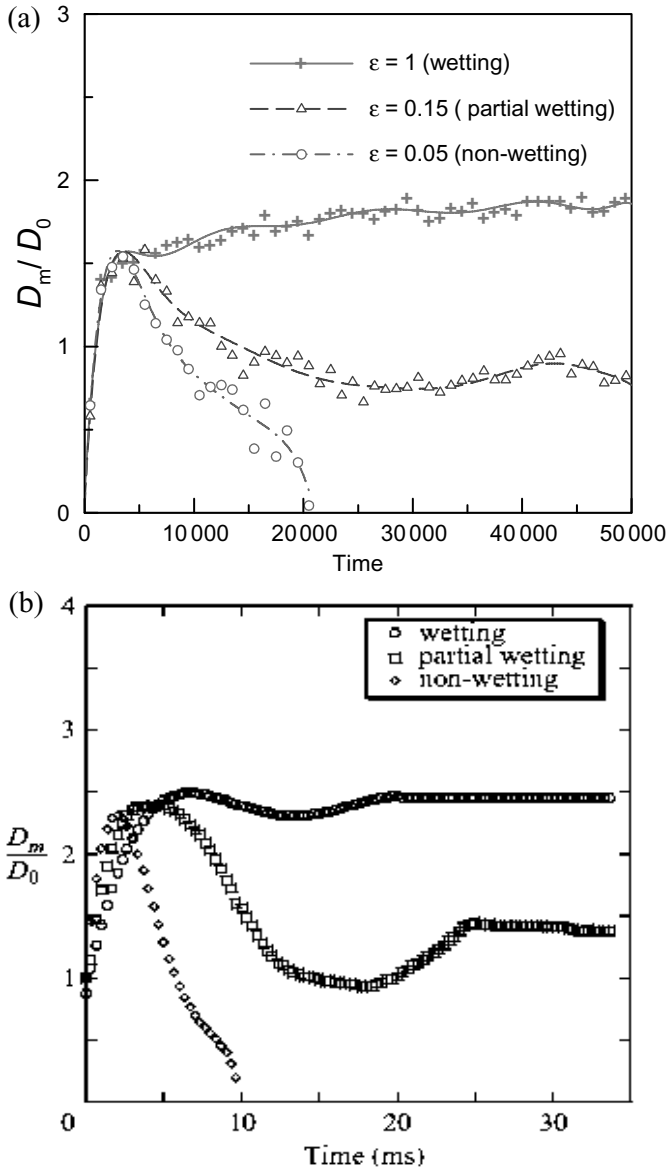

Figure 3. Temporal variation of the normalized spreading diameter of droplets impacting on solid surfaces with different wetting characteristics: (a) simulations for a 6 nm droplet with initial velocity, $V_0 = 1.25\,\mathrm{m\,s^{-1}}$, (b) experimental results (from Bayer and Megaridis 2006) for a 1.4 mm water droplet with initial velocity $V_0 = 0.77\,\mathrm{m\,s^{-1}}$. For simulations, time is given in number of time steps, with step size $\Delta t = 1.078 \times 10^{-14}$ s.

the contact angle[6] decreases slowly and approaches its equilibrium value (cf figure 5). The simulations reproduce this process also reasonably well. The simulations, however, do not capture the surface capillary waves, propagating from the solid wall to the top of the drop,

[6] The temporal variation of contact angle for different surfaces is discussed in the next section.

observed in the experimental study. This may be due to the extremely small length and time scales used in simulations, and needs to be investigated in a future study.

Results in figures 1–3 further indicate that the spreading process during the receding stage is strongly influenced by surface wettability. Both the simulations and experiments indicate that for partially wettable and non-wettable surfaces, the receding stage is characterized by the decrease in spreading diameter or retraction of the contact line. This is clearly indicated by the experimental images at 10.6, 15.4 and 21.4 ms for the partially wettable surface, and at 6.6, 10.2 and 11.4 ms for the non-wettable surface in figure 2. The simulations also produce this overall behavior, as indicated by images at 8500, 14 500 and 17 000 steps for the partially wettable surface, and at 6000, 12 000 and 21 000 steps for the non-wettable surface in figure 1. There are, however, differences between simulations and experiments with respect to the droplet shape and the oscillations observed in experiments. As shown in figures 1–3, the experimentally observed variation in droplet shape and spreading diameter during the receding period is not well captured by simulations. Moreover, simulations are not able to reproduce the surface capillary waves observed in experiments. This may be due to the extremely small length and time scales used in simulations, as noted earlier. The spreading near the end of the receding stage is characterized by the contact diameter approaching its equilibrium value for the partially wettable surface, while it involves droplet bounce-off for the non-wettable surface. The liquid separation from the surface and the droplet bouncing from the non-wettable surface can be seen in the experimental image at 15.8 ms (figure 2), and at 28 500 steps in simulations (figure 1). These receding and bouncing processes observed in our simulations are also consistent with the results reported by Ok *et al* (2004) for continuum-size droplets.

The similarity between our simulations and reported experiments is further examined using the relevant characteristic times associated with the advancing, receding and bouncing processes. The advancing, receding and bounce-off times obtained from the experiments and simulations are listed in tables 2(b)–(d), respectively. Note that the experimental values are only approximate, as these were estimated from figures 2 and 3. Since the time and lengths scales are vastly different between simulations and reported experiments, the relevant characteristic times may be computed based on the consideration that the spreading process is governed by inertial, viscous and surface forces. This yields the following two characteristic time scales:

$$t_{c1} = \mu D_o/\gamma, \quad t_{c2} = \rho D_o^2 V/\gamma$$

The first time scale (t_{c1}) considers viscous and surface forces, while the second (t_{c2}) considers inertial and surface forces. Here V and D_o are the droplet impact velocity and diameter, respectively, and μ, ρ and γ are the liquid viscosity, density and surface tension, respectively. The values of t_{c1} and t_{c2} for the water (experiments) and argon[7] (simulations) droplets are listed in table 2(a). Due to the vastly different scales used in experiments and simulations, it is relevant to compare the ratio of various time scales. The ratios of t_{c1} and t_{c2}, termed as t_{R1} and t_{R2}, are shown in table 2(a), while those of the advancing, receding and bouncing times in experiments and simulations are shown in tables 2(b)–(d), respectively. As indicated in these tables, the ratios of the advancing, receding and bouncing times for the three surfaces and three droplet sizes vary within a factor of three. More importantly, these ratios differ from t_{R2} (ratio of the experimental and computational characteristic times based on inertial and surface forces) by about an order of magnitude, while they differ from t_{R1} (ratio of the experimental and computational characteristic times based on viscous and surface forces) by three orders of magnitude. Thus the comparison indicates that the spreading process is governed by inertial

[7] The argon properties were calculated using the NIST database.

Table 2. Comparison of characteristic times in simulations and experiments (Bayer and Megaridis 2006).

(a) Characteristic times (t_{c1} and t_{c2}) and their ratios.

Experiment			Simulation				
D (mm)	t_{c1} (s)	t_{c2} (s)	D (nm)	t_{c1} (s)	t_{c2} (s)	$t_{R1} = \frac{(t_{c1})_{exp}}{(t_{c1})_{sim}}$	$t_{R2} = \frac{(t_{c2})_{exp}}{(t_{c2})_{sim}}$
1.4	1.93×10^{-5}	1.88×10^{-2}	6	1.30×10^{-10}	4.53×10^{-12}	1.48×10^{5}	4.16×10^{9}
1.4	1.93×10^{-5}	1.88×10^{-2}	9	1.95×10^{-10}	1.02×10^{-11}	9.89×10^{4}	1.85×10^{9}
1.4	1.93×10^{-5}	1.88×10^{-2}	12	2.60×10^{-10}	1.81×10^{-11}	7.42×10^{4}	1.04×10^{9}

(b) Advancing times in experiments and simulations (wettable surface).

Experiment		Simulation			
	Advancing time		Advancing time		
D (mm)	t_{exp} (s)	D (nm)	(# steps)	t_{sim} (s)	$\frac{t_{exp}}{t_{sim}}$
1.4	4.20×10^{-3}	6	5000	5.39×10^{-11}	7.79×10^{7}
1.4	4.20×10^{-3}	9	8000	8.62×10^{-11}	4.87×10^{7}
1.4	4.20×10^{-3}	12	10000	1.08×10^{-10}	3.90×10^{7}

(c) Receding time in experiments and simulations (partially wettable surface).

Experiment		Simulation			
	Receding time		Receding time		
D (mm)	t_{exp} (s)	D (nm)	(# steps)	t_{sim} (s)	$\frac{t_{exp}}{t_{sim}}$
1.4	1.54×10^{-2}	6	25 000	2.70×10^{-10}	5.71×10^{7}
1.4	1.54×10^{-2}	9	30 000	3.23×10^{-10}	4.76×10^{7}
1.4	1.54×10^{-2}	12	37 000	3.99×10^{-10}	3.86×10^{7}

(d) Bouncing time in experiments and simulations (non-wettable surface).

Experiment		Simulation			
	Bouncing time		Bouncing time		
D (mm)	t_{exp} (s)	D (nm)	(# steps)	t_{sim} (s)	$\frac{t_{exp}}{t_{sim}}$
1.4	1.34×10^{-2}	6	28 000	3.02×10^{-10}	4.44×10^{7}
1.4	1.34×10^{-2}	9	46 000	4.96×10^{-10}	2.70×10^{7}
1.4	1.34×10^{-2}	12	80 000	8.62×10^{-10}	1.55×10^{7}

and surface forces rather than by viscous forces, and on this basis, there is noticeable similarity between experiments and simulations.

The present results are also generally consistent with those reported in some previous studies (Rioboo *et al* 2002, Heine *et al* 2003). For instance, experiments of Rioboo *et al* (2002) yield the variation of D_m/D_0 with time as $D_m/D_0 \propto t^{0.453\pm0.005}$, while those of Bayer and Megaridis (2006) yield as $t^{0.5}$, and the MD simulations of Heine *et al* (2003) give $D_m/D_0 \propto t^{0.46\pm0.03}$. Our simulations yield $D_m/D_0 \propto t^{0.63\pm0.04}$.

3.2. Effect of drop size on spreading dynamics

Figure 4 depicts spreading dynamics in terms of the computed images for a 12 nm droplet on wettable, partially wettable and non-wettable surfaces. In order to examine the effect of

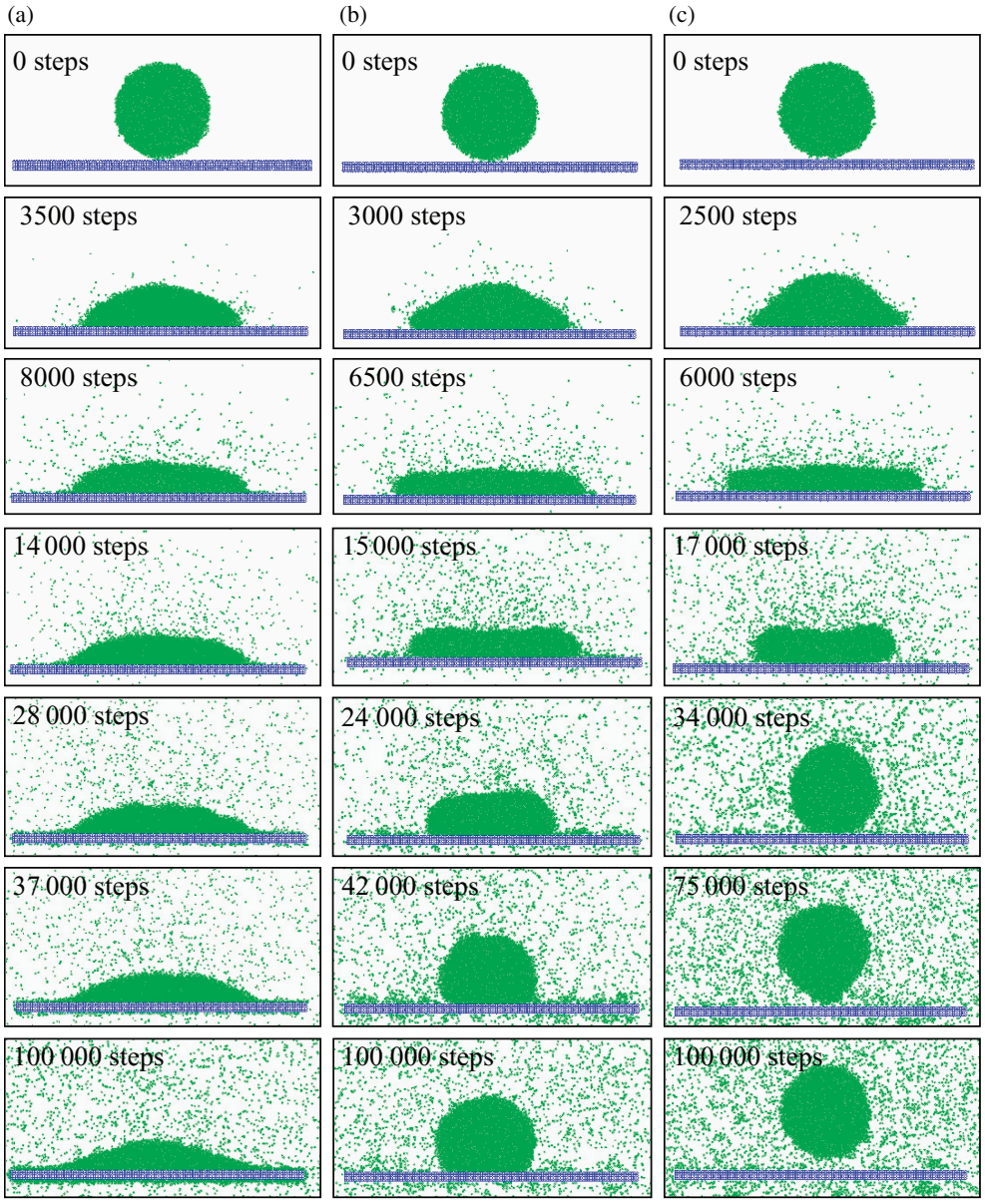

Figure 4. Spreading dynamics of 12 nm droplets with initial velocity $V_0 = 1.25\,\mathrm{m\,s^{-1}}$ on three flat surfaces with different wetting characteristics: (a) wettable surface, $\varepsilon_w = 1.0$, (b) partially wettable, $\varepsilon_w = 0.15$ and (c) non-wettable, $\varepsilon_w = 0.05$.

droplet size on the spreading behavior, it is instructive to compare these images with the corresponding images for the 6 nm droplet presented in figure 1. While the spreading process appears to be qualitatively similar for the two droplets, there are significant quantitative differences. The dynamic contact angle and spreading diameter, as well as the advancing and receding time periods, are noticeably different for the two droplets, indicating size dependence of the spreading process. More quantitative results from our simulations are presented in figures 5–7, which show the temporal variation of contact angle and spreading diameter

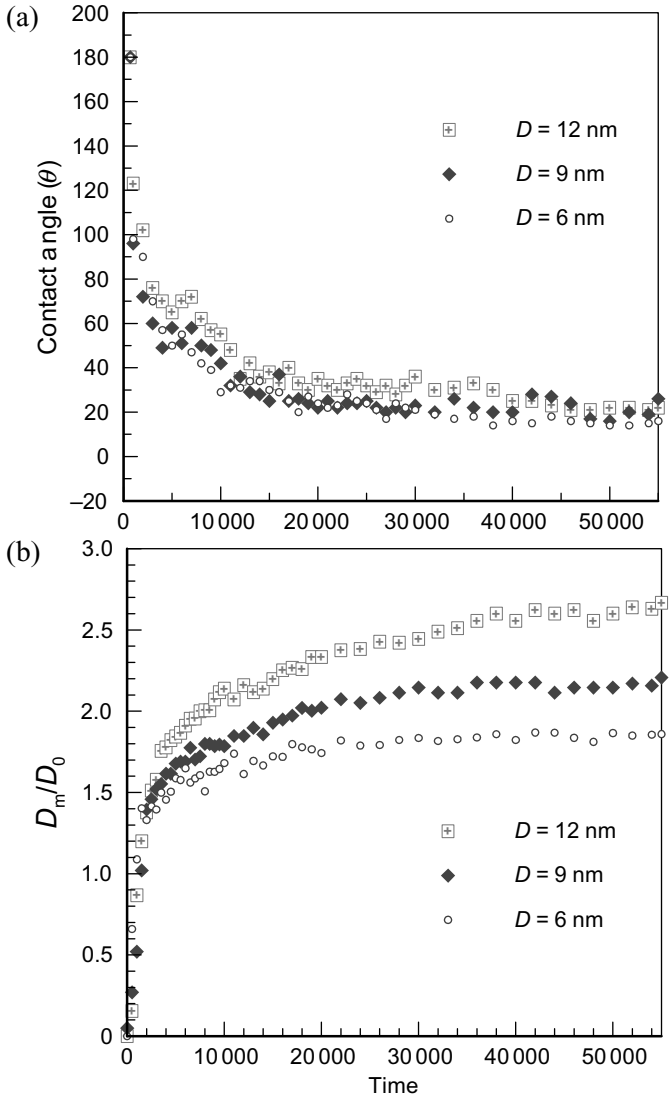

Figure 5. Temporal evolution of (a) dynamic contact angle and (b) normalized spreading diameter for three different droplet sizes for spreading on a wettable surface ($\varepsilon_w = 1.0$). The initial impact velocity is $V_0 = 1.25\,\mathrm{m\,s^{-1}}$. Time is given in terms of the number of time steps, with step size $\Delta t = 1.078 \times 10^{-14}$ s.

for the 6, 9 and 12 nm droplets impinging on wettable, partially wettable and non-wettable surfaces, respectively. As stated earlier, the algorithm for computing the instantaneous contact angle is based on tracking the liquid–vapor interface (Sedighi *et al* 2009). It should also be noted that the uncertainty or error in the computation of contact angle and spreading diameter ranged between 5–12% and 4–10% depending upon the surface wettability. Consistent with the images shown in figures 1 and 4, as the droplet spreads on a wettable surface, the contact angle decreases rapidly from 180° to almost 20° during the advancing stage, and slowly approaches its equilibrium value (cf figure 5(a)). Similarly, the spreading diameter increases

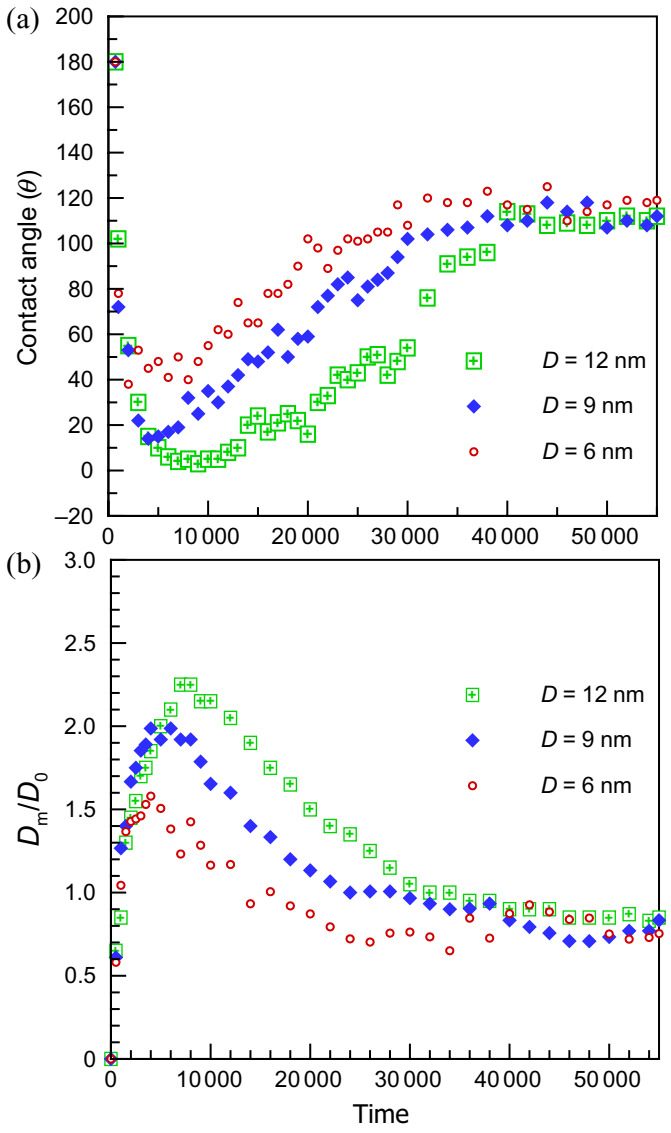

Figure 6. Temporal evolution of (a) dynamic contact angle and (b) normalized spreading diameter for three different droplet sizes for spreading on a partially wettable surface ($\varepsilon_w = 0.15$). Time is given in terms of the number of time steps, with step size $\Delta t = 1.078 \times 10^{-14}$ s.

rapidly during the advancing stage, and then becomes nearly constant or continues to increase at a much slower rate (for 12 nm droplet) as it approaches the equilibrium state. Thus while the equilibrium contact angle is independent of the droplet size, the dynamic contact angle and spreading diameter are strongly size dependent.

Figures 6 and 7 present the variation of dynamic contact angle and spreading diameter for the partially wettable and non-wettable surfaces, respectively. As noted earlier, the spreading process on such surfaces can be divided into two main stages: advancing and receding. The spreading dynamics during the advancing stage is essentially independent of the surface

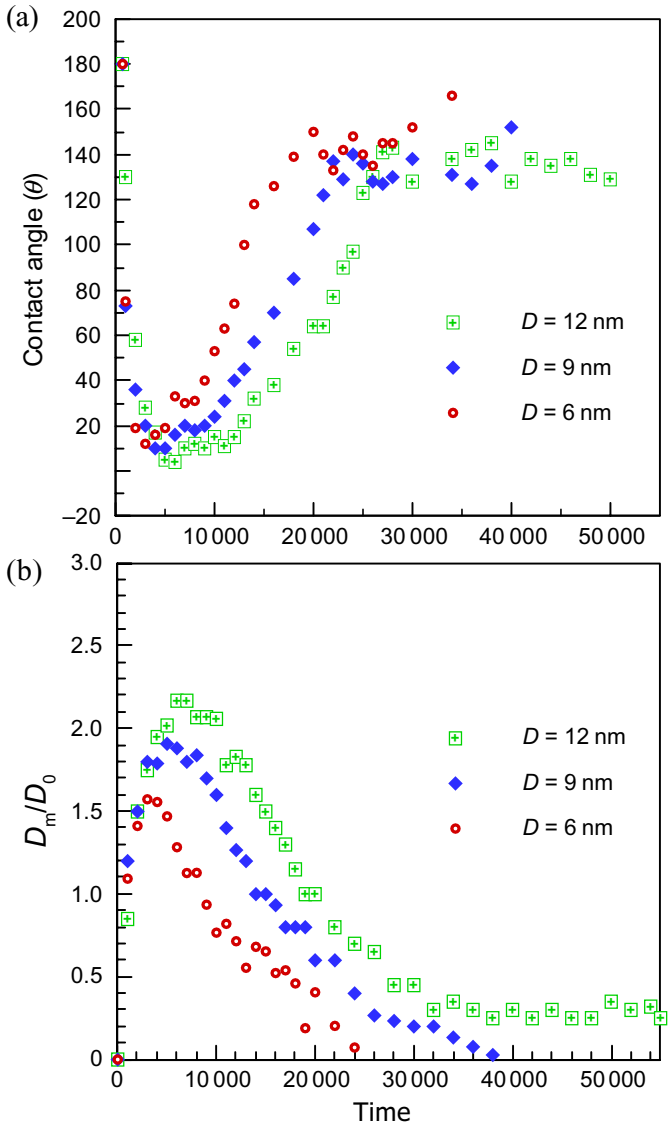

Figure 7. Temporal evolution of (a) dynamic contact angle and (b) normalized spreading diameter for three different droplet sizes spreading on a non-wettable surface ($\varepsilon_w = 0.05$). Time is given in terms of the number of time steps, with step size $\Delta t = 1.078 \times 10^{-14}$ s.

wetting properties. During this stage, the contact angle decreases while the spreading diameter increases rapidly. During the receding stage, the droplet recoils, characterized by an increase in contact angle and a corresponding decrease in spreading diameter with time. The spreading during this stage is strongly influenced by both the surface wettability and droplet size. For a partially wettable surface, the contact angle approaches its equilibrium value as determined by the surface wetting characteristics, while for a non-wettable surface, the contact angle essentially returns to 180°, implying that the droplet rebounds from the surface. This is also indicated by the spreading diameter, which decreases to zero for the non-wettable surface

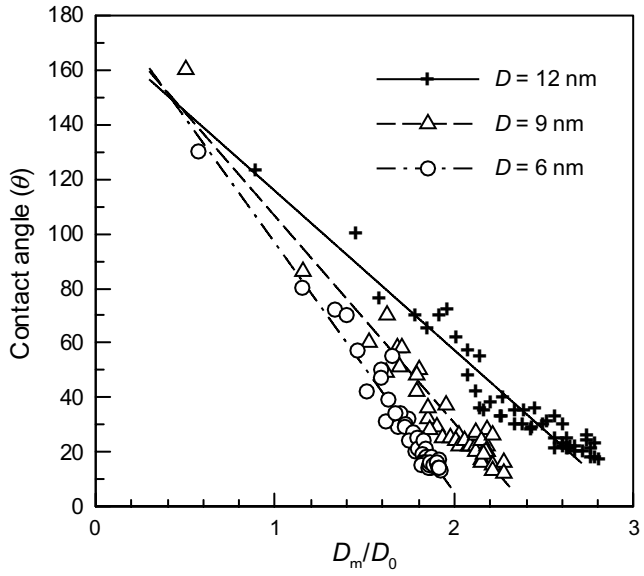

Figure 8. Dynamic contact angle plotted versus spreading diameter for a wettable surface ($\varepsilon_w = 1.0$).

(cf figure 7(a)), as the contact area takes the form of a neck that connects the droplet to the surface (figure 1). The droplet oscillates around its neck for a short period and then rebounds from the surface. Another effect of surface wettability is that the receding period is longer than the advancing period for the partially wettable surface, but is nearly the same as the advancing period for the non-wettable surface. This is expected, since the reduced wettability implies decreased interaction between the liquid and solid surface.

Further, our results (cf figures 5–7) indicate strong correlation between dynamic contact angle and spreading diameter. This can be seen more clearly in figures 8 and 9, which show the dynamic contact angle variation with the normalized spreading diameter. Results for the wettable surface indicate almost a linear relationship between contact angle and spreading diameter for all three droplet sizes. However, the slope of the plot depends on the droplet size, and increases as the droplet size decreases, implying an inertia-dominated spreading process. For a partially wettable surface, the correlation between contact angle and spreading diameter is linear during the advancing stage, but exhibits nonlinear behavior during the receding stage (cf figure 9). Moreover, hysteresis is observed for both the partially wettable and non-wettable surfaces, and becomes somewhat more pronounced for larger droplets. The hysteresis phenomenon has been observed in several previous studies and has been discussed by Blake (2006).

3.3. Scaling relationships for dynamic spreading characteristics

An important observation from figures 5–7 is that the dynamic spreading process is influenced by droplet size. The dynamic contact angle and spreading diameter exhibit strong dependence on droplet size irrespective of the surface wetting characteristics. The characteristic times associated with advancing and receding stages are also influenced by droplet size. In order to obtain scaling relationships for the effect of droplet size on these spreading parameters,

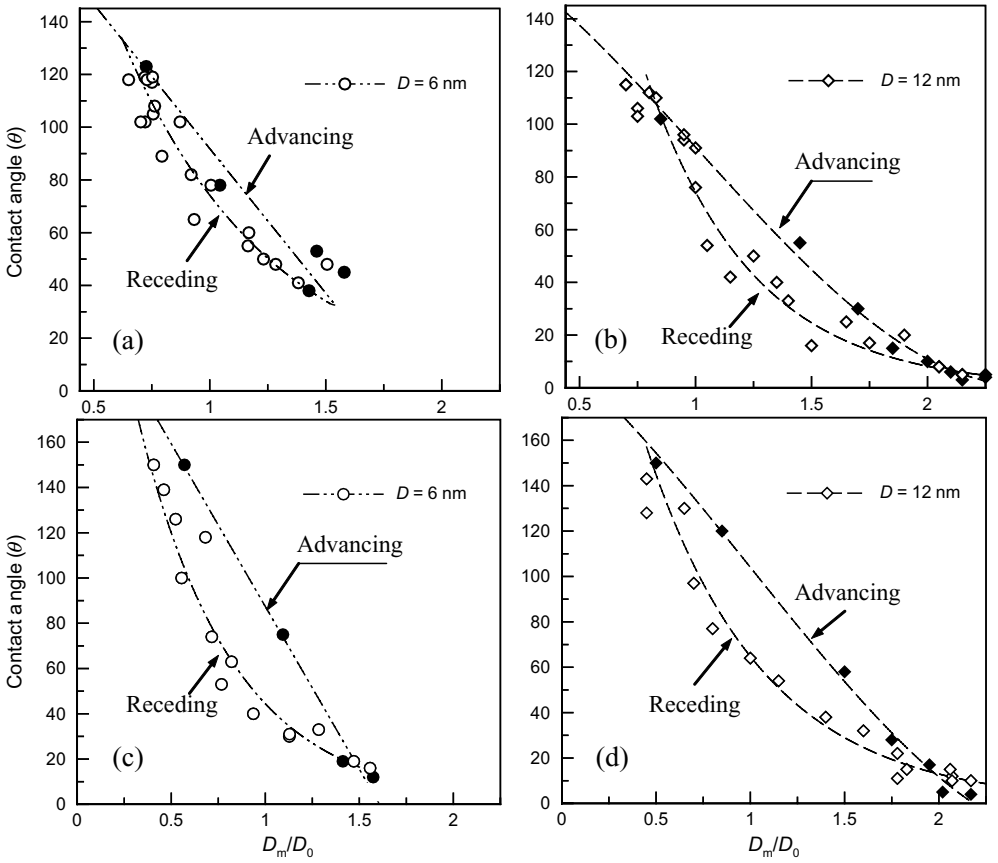

Figure 9. Dynamic contact angle plotted versus spreading diameter during the advancing and receding stages for partially wettable ($\varepsilon_w = 0.15$) ((a) and (b)) and non-wettable ($\varepsilon_w = 0.05$) ((c) and (d)) surfaces.

we analyzed the simulation results, which yielded the following relation for the spreading diameter, $D_m(t)$. An analysis of the theoretical basis of the observed size dependence also follows in sections 3.4.

$$D_m/D_0 \propto D_0^{0.5} \quad \text{or} \quad \frac{(D_m/D_o)_2}{(D_m/D_o)_1} = (D_{o2}/D_{o1})^{0.5}. \tag{2}$$

Similarly the effect of droplet size on dynamic contact angle was given by the following correlation[8]:

$$\theta_R \propto D_0^{0.5} \quad \text{or} \quad \theta_{R2}/\theta_{R1} = (D_{o2}/D_{o1})^{0.5}. \tag{3}$$

The rescaled contact angle θ_R is defined as

$$\theta_R = \theta - \theta_A. \tag{4}$$

[8] The equilibrium contact angle was, however, found to be independent of droplet size, as it only varied with the surface wettability.

Here θ_A is the contact angle at the end of advancing period. The scaling for the dynamic contact angle is based on the consideration that the contact angle exhibits a linear relationship with the spreading diameter, especially in the advancing stage. The above correlations were found to hold for the three wettable, partially wettable and non-wettable surfaces investigated. Further, the simulations yielded the following correlation for the advancing and receding time periods:

$$t \propto D_0^{2/3} \quad \text{or} \quad t_2/t_1 = (D_{o2}/D_{o1})^{2/3}. \tag{5}$$

Subscript 1 in the above equations refers to the 12 nm droplet. Note that a similar time dependence was obtained for D_m/D_o in section 3.1. Figures 10–12 present the observed results for rescaled contact angle and spreading diameter (based on equations (2) and (3)) plotted versus the rescaled time (equation (5)) for the wettable, partially wettable and non-wettable surfaces, respectively. These plots clearly demonstrate the validity of the above correlations, except for some variances during the receding stage for the partially wettable and non-wettable surfaces. For comparison these rescaled plots should be compared with figures 5–7 on a one–one basis.

3.4. Additional analysis of scaling relationships

An attempt was also made to provide the physical basis and further validation for the above scaling relationships. One can obtain a scaling relation for the spreading diameter by assuming that during spreading the droplet shape changes from a sphere to a flattened sphere, and in this process the droplet kinetic energy is dissipated by viscous effects. This yields the following:

$$\rho D_0^3 V_0^2 \propto \mu (V_0/h) D_m^3, \tag{6}$$

where h is the thickness of the flattened drop corresponding to its maximum spreading position. Using the conservation of volume during this process, i.e. $D_0^3 \propto h D_m^2$, yields the scaling relation as $D_m/D_o \propto Re^{1/5}$, as discussed in Chandra and Avedisian (1991) and Rein (1993), or $D_m/D_o \propto D_o^{1/5}$. Since the present simulations indicate $D_m/D_o \propto D_o^{1/2}$, the viscous effects may not be as significant for sub-micron droplets, especially for partially wettable and non-wettable surfaces. Therefore, assuming that the droplet spreading process is analogous to the stretching and recoiling of a spring, and its kinetic energy is converted to surface energy (Richard *et al* 2002) yields

$$\rho D_0^3 V_0^2 \equiv \gamma D_m^2 \tag{7}$$

Since the liquid density and initial droplet velocity were kept the same for different droplet sizes investigated, this leads to the correlation given by equation (2), i.e.

$$D_m/D_0 \propto D_0^{0.5} \quad \frac{(D_m/D_o)_2}{(D_m/D_o)_1} = (D_{o2}/D_{o1})^{0.5}. \tag{8}$$

Thus, the present MD results indicate that the hypothesis based on surface energy is more meaningful than that based on viscous dissipation for the spreading of nano-size droplets. It is also important to compare our correlations with those reported in the literature. Sikalo *et al* (2002) reported experimental data for isopropanol droplets with diameters of 3.3 and 1.8 mm, which indicated a smaller spreading diameter for the smaller droplet. However, they suggested that the viscous effect is more important. Previous studies have reported correlations for the maximum spreading diameter for macroscopic droplets. Several of these correlations are listed in table 1 of Bathel *et al* (2007). It is difficult, however, to compare our results with those in table 1, since the droplet diameter is embedded in the Weber number

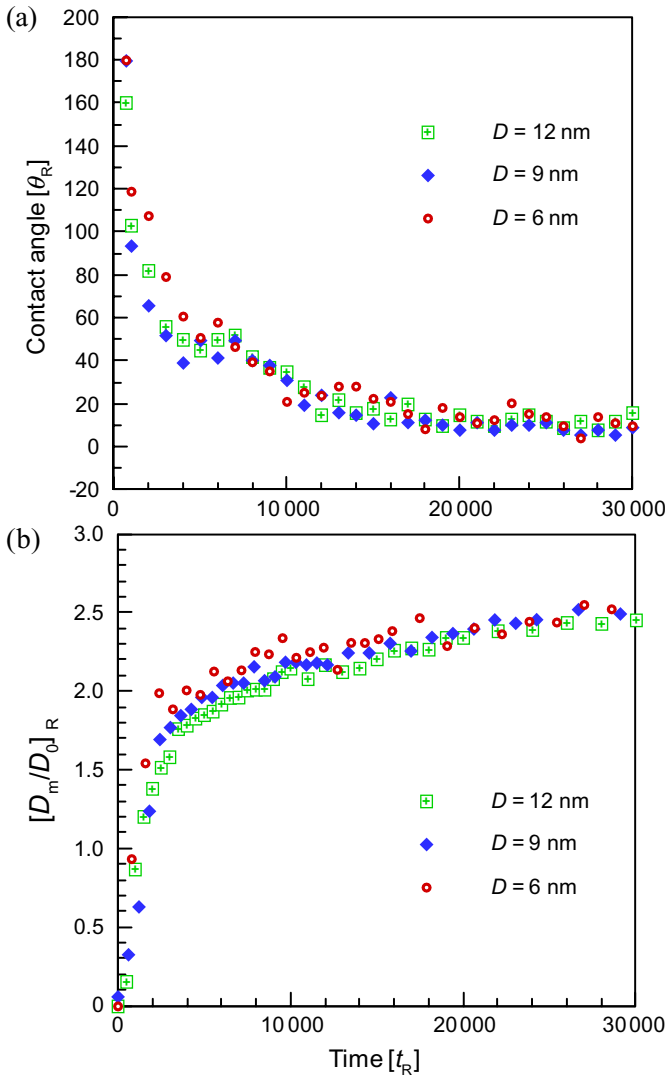

Figure 10. Rescaled (a) contact angle and (b) spreading diameter plotted versus rescaled time for three different-size droplets spreading on a wettable surface ($\varepsilon_w = 1.0$).

and Reynolds number. However, the correlation of Scheller and Bousfield (1995) provides a more direct variation with the droplet size, yielding $D_m/D_0 \propto D_0^{0.25}$. Comparison with our correlation suggests that viscous effects are relatively more important for large droplets.

The dependence of advancing or spreading time on the droplet size, as given by equation (5), may be analyzed by considering the free energy of the system. Defining a characteristic time in terms of the mass (m), characteristic length (D) and free energy (E) as

$$t = (mD^2/E)^{1/2} \quad \text{or} \quad t \propto D_0^{5/2} E^{-1/2}, \quad \text{since } m \propto D_0^3. \tag{9}$$

The expression for the system free energy E follows the formulation of Fan (2006), and is given by

$$E = \gamma_{lv} A_{lv} + \gamma_{sl} A_{sl} + \gamma_{sv} A_{sv} + \tau L - W. \tag{10}$$

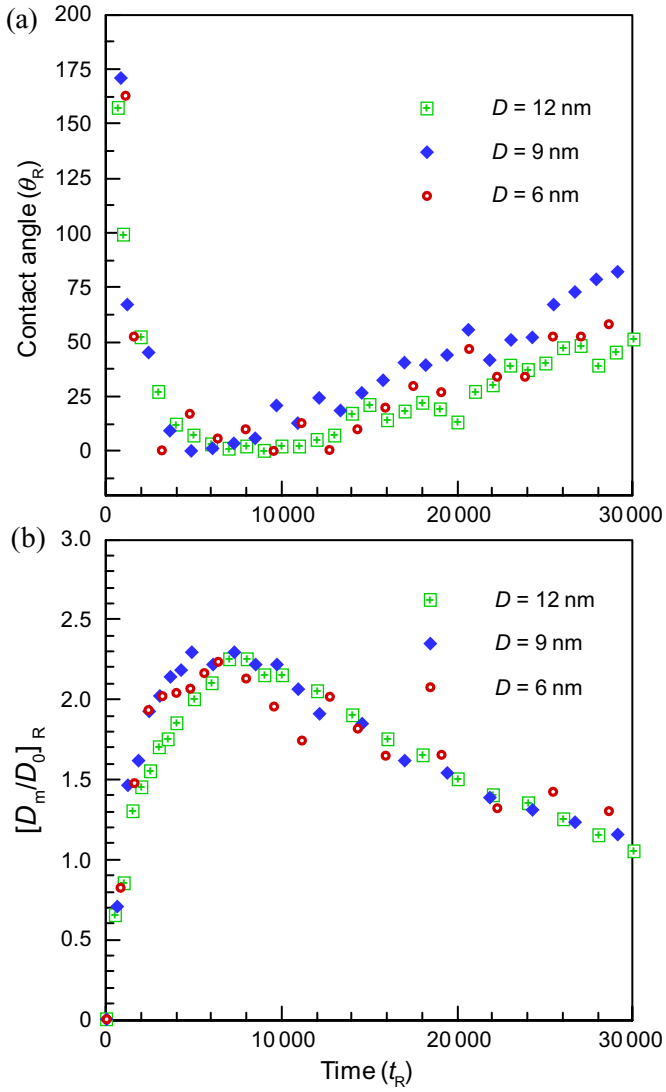

Figure 11. Rescaled (a) contact angle and (b) spreading diameter plotted versus rescaled time for three different-size droplets spreading on a partially wettable surface ($\varepsilon_w = 0.15$).

The first three terms in the above equation represent the surface energy, L is the line tension of the three-phase line and W the external work supplied to the system. Following Widom (1995), the above equation can be written as

$$E = 2\pi R^2[\gamma_{lv}(1+\cos\theta) + (1/2)(\gamma_{sl}-\gamma_{sv})(\sin\theta)^2 + \tau(\sin\theta)/R + \Delta p(R\sin\theta)(1+\cos\theta)]. \tag{11}$$

Here R is the spreading radius and θ the contact angle. In order to obtain a simplified scaling equation, we neglect the contributions of line tension and external work, represented by the last two terms in the above equation. Consequently, $E \propto R^2$ or $E \propto D_m^2$, which

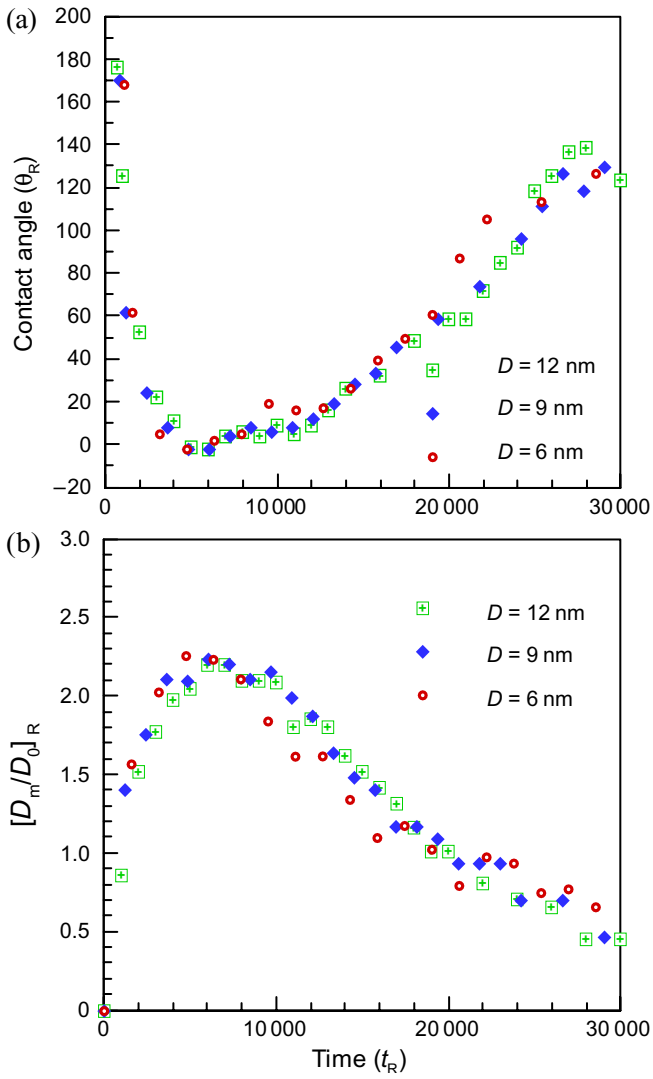

Figure 12. Rescaled (a) contact angle and (b) spreading diameter plotted versus rescaled time for three different-size droplets spreading on a non-wettable surface ($\varepsilon_w = 0.05$).

leads to

$$t \propto D_o. \tag{12}$$

Simulations, however, yield $t \propto D_o^{2/3}$. As discussed by Fan (2006), the effect of line tension may not be negligible for micron and nanometer droplets. Consequently, a more general scaling for the spreading time may be written as

$$t \propto D_o^n \quad \text{where } n < 1. \tag{13}$$

It is also interesting to note that using D_m as the characteristic length (instead of D_o in equation (9)) would yield $t \propto D_o^{3/2}$, which is consistent with the time scale associated with the drop oscillation frequency (Clift *et al* 1978, Richard *et al* 2002).

4. Conclusions

MD simulations have been performed to investigate the spreading behavior of nano-size droplets impinging on flat surfaces. The effect of droplet size on spreading dynamics has been characterized for wettable, partially wettable and non-wettable surfaces. The computational model has been validated through a qualitative comparison with the measurements of Bayer and Megaridis (2006), and comparison with existing correlations. The comparison with measurements, based on the ratio of the relevant time scales, also indicates that for the conditions investigated, the spreading dynamics is governed by the inertial and surface forces, with negligible influence of the viscous forces.

Results indicate that the spreading dynamics is strongly influenced by the droplet size. The dynamic contact angle and spreading diameter, as well as the advancing and receding time periods, exhibit strong dependence on droplet size irrespective of the surface wetting characteristics. Simulation results have been analyzed to develop correlations for the effect of droplet size on these spreading parameters. The correlations indicate that the normalized spreading diameter and contact angle scale with drop diameter as $D_m/D_0 \propto D_0^{0.5}$ and $\theta_R \propto D_0^{0.5}$, while the advancing and receding time periods scale as $t \propto D_0^{2/3}$. We have also used global energy considerations to provide a physical basis for these correlations.

While the present simulations for nano-size droplets exhibit good qualitative and reasonable semi-quantitative comparison with measurements for continuum-size droplets, additional experimental and computational studies are needed to provide more quantitative validation for the correlations developed in the present study. Experimental studies should focus on providing time-resolved measurements of the spreading process for micron- and nano-size droplets, while MD simulations should consider more realistic fluids and surfaces, as well as larger droplets.

Acknowledgments

We thank Professor Ludwig Nitsche for helpful discussions. SM was supported in part from a grant from the Office of Basic Energy Sciences, US Department of Energy (DE-FG02-08ER46538)

References

Allen M P and Tildesley D J 1987 *Computer Simulation of Liquids* (Oxford: Clarendon)

Asai A, Shiova M, Hirasawa S and Okazaki T 1993 Impact of an ink drop on paper *J. Imaging Sci. Technol.* **37** 205–7

Attinger D, Zhao Z and Poulikakos D 2000 An experimental study of molten microdroplet surface deposition and solidification: transient behavior and wetting angle dynamics *J. Heat Transfer* **122** 544–56

Aziz S D and Chandra S 2000 Impact, recoil and splashing of molten metal droplets *Int. J. Heat Mass Transfer* **43** 2841–57

Bathel B F, Stephen N, Johnson L and Ratner A 2007 Prediction of postcontact parameters of fluid droplet impact on a smooth surface *AIAA J.* **45** 1725–33

Bayer I S and Megaridis C M 2006 Contact angle dynamics in droplets impacting on flat surfaces with different wetting characteristics *J. Fluid Mech.* **558** 415–49

Blake T D 2006 The physics of moving wetting lines *J. Colloid Interface Sci.* **299** 1–13

Blake T D and Haynes J M 1969 Kinetics of liquid/liquid displacement *J. Colloid Interface Sci.* **30** 421–3

Boland T, Tao X, Damon B J, Manley B, Kesari P, Jalota S and Bhadur S 2007 Drop-on-demand printing of cells and materials for designer tissue constructs *Mater. Sci. Eng.* C **27** 372–6

Cazabat A M, Fraysse N and Heslot F 1990 Molecular wetting films *Prog. Colloid Polym. Sci.* **83** 52–5

Chandra S and Avedisian C T 1991 On the collision of a droplet with solid surface *Proc. R. Soc.* A **432** 13–41

Cherry B W and Holmes C M 1969 Kinetics of wetting of surfaces by polymers *J. Colloid Interface Sci.* **29** 174–6
Choi T Y, Poulikakos D and Grigoropoulos C P 2004 Fountain-pen-based laser microstructuring with gold nanoparticle inks *Appl. Phys. Lett.* **85** 13–5
Clift R, Grace J R and Weber M E 1978 *Bubbles, Drops and Particles* (New York: Academic Press)
Cox R G 1986 The dynamics of the spreading of liquids on a solid surface *J. Fluid Mech.* **168** 169–94
Crooks R, Cooper-White J and Boger D V 2001 The role of dynamic surface tension and elasticity on the dynamics of drop impact *Chem. Eng. Sci.* **56** 5575–92
De Coninck J, D'Ortona U, Koplik J and Banavar J 1995 Terraced spreading of chain molecules via molecular dynamics *Phys. Rev. Lett.* **74** 928–31
De Coninck J, De Ruijter M J and Voue M 2001 Dynamics of wetting *Curr. Opin. Colloid Interface Sci.* **6** 49–53
de Gennes P G 1985 Wetting: statics and dynamics *Rev. Mod. Phys.* **57** 827–63
Delplanque J P and Rangel R H 1997 An improved model for droplet solidification on a flat surface *J. Mater. Sci.* **32** 1519–30
Dong H, Carr W W and Morris J F 2006 Visualization of drop-on-demand inkjet: drop formation and deposition *Rev. Sci. Instrum.* **77** 085101
Dussan E B 1979 On the spreading of liquid on solid surface: static and dynamic contact angle *Ann. Rev. Fluid Mech.* **11** 371–400
Fan H 2006 Liquid droplet spreading with line tension effect *J. Phys.: Condens. Matter* **18** 4481–8
Graham-Rowe D 2007 Medicine—Ultrasonic tourniquet *Technol. Rev.* **109** 15
Heine D R, Grest G S and Webb E B III 2003 Spreading dynamics of polymer nanodroplets *Phys. Rev.* E **68** 061603
Heslot F, Fraysse N and Cazabat A M 1989 Molecular layering in the spreading of wetting liquid drops *Nature* **338** 640–2
Hoffman R H 1975 A study of the advancing interface 1. interface shape in liquid-gas systems *J. Colloid Interface Sci.* **50** 228–41
Kim H Y, Park S Y and Min K 2003 Imaging the high-speed impact of microdrop on solid surface *Rev. Sci. Instrum.* **74** 4930–7
Lee D H, Chang Y J, Herman G S and Chang C H 2007 A general route to printable high-mobility transparent amorphous oxide semiconductors *Adv. Mater.* **19** 843–7
Lee J and Kim C J 2000 Surface-tension-driven microactuation based on continuous electrowetting *J. Microelectromech. Syst.* **9** 2 171–80
Mao T, Kuhn D C S and Tran H 1997 Spread and rebound of liquid droplets upon impact on flat surfaces *AIChE J.* **43** 2169–79
Ok H, Park H, Carr W W, Morris J F and Zhu J 2004 Particle-laden drop impacting on solid surfaces *J. Dispers. Sci. Technol.* **25** 449–56
Pasandideh-Fard M, Qiao Y M, Chandra S and Mostaghimi J 1996 Capillary effects during droplet impact on a solid surface *Phys. Fluids* **8** 650–9
Pede D, Serra G and De Rossi D 1998 Microfabrication of conducting polymer devices by ink-jet stereolithography *Mater. Sci. Eng.* C **5** 289–91
Rein M 1993 Phenomena of liquid drop impact on solid and liquid surface *Fluid Dyn. Res.* **12** 61–93
Richard D, Clanet C and Quere D 2002 Surface phenomena—contact time of a bouncing drop *Nature* **417** 811
Rioboo R, Marengo M and Tropea C 2002 Time evolution of liquid drop impact onto solid, dry surfaces *Exp. Fluids* **33** 112–4
de Ruijter M, Blake T D, Clarke A and De Coninck J 1999 Droplet spreading: a tool to characterize surfaces at the microscopic scale *J. Petrol. Sci. Eng.* **24** 189–98
Scheller B and Bousfield D W 1995 Newtonian drop impact with a solid surface *AIChE J.* **41** 1357–67
Sedighi N, Murad S and Aggarwal S K 2009 Molecular dynamics simulations of nano-droplet wetting on a solid surface *Atom. Sprays* **19** 11–5
Shikhmurzaev Y D 1997 Moving contact lines in liquid/liquid/solid systems *J. Fluid Mech.* **334** 211–49
Sikalo S, Marengo M, Tropea C and Ganic E N 2002 Analysis of impact of droplets on horizontal surfaces *Exp. Therm. Fluid Sci.* **25** 503–10
Starov V M, Zhdanov S A and Velarde M G 2002 Spreading of liquid drops over thick porous layers: complete wetting case *Langmuir* **18** 9744–50
Tanner L H 1979 Spreading of silicone oil drops on horizontal surfaces *J. Phys. D: Appl. Phys.* **12** 1473–84
Van Dam D B and Le Clerc C 2004 Experimental study of the impact of an ink-jet printed droplet on a solid substrate *Phys. Fluids* **16** 3403–14
Voue M, De Coninck J, Villette S, Valignat M P and Cazabat A M 1998a Investigation of layered microdroplets using ellipsometric techniques *Thin Solid Films* **313–314** 819–24

Voue M, Valignat M P, Oshanin G, Cazabat A M and De Coninck J 1998b Dynamics and spreading of liquid microdroplets on substrates of increasing surface energy *Langmuir* **14** 5951–8

Widom B 1995 Line tension and the shape of a sessile drop *J. Phys. Chem.* **99** 2803–6

Yang J X, Koplik J and Banavar J 1991 Molecular dynamics of drop spreading on a solid surface *Phys. Rev. Lett.* **67** 3539–42

Yang W J 1995 Theory on vaporization and combustion of liquid drops of pure substances and binary mixtures on heated surfaces *Technical Report* **535** Institute of Space and Aeronautical Science, University of Tokyo

Yarin A L 2006 Drop impact dynamics: splashing, spreading, receding, bouncing *Ann. Rev. Fluid Mech.* **38** 159–92

Zhao Z, Poulikakos D and Fukai J 1996 Heat transfer and fluid dynamics during the collision of a liquid droplet on a substrate 1. Modeling *Int. J. Heat Mass Transfer* **39** 2771–89